

Supplement of

# **Rethinking the role of transport and photochemistry in regional ozone pollution: Insights from ozone concentration and mass budgets**

Kun Qu<sup>1,2,3</sup>, Xuesong Wang<sup>1,2</sup>, Xuhui Cai<sup>1,2</sup>, Yu Yan<sup>1,2</sup>, Xipeng Jin<sup>1,2</sup>, Mihalis Vrekoussis<sup>3,4,5</sup>, Jin Shen<sup>6</sup>, Teng Xiao<sup>1,2</sup>, Limin Zeng<sup>1,2</sup>, and Yuanhang Zhang<sup>1,2,7,8</sup>

<sup>1</sup>State Key Joint Laboratory of Environmental Simulation and Pollution Control, College of Environmental Sciences and Engineering, Peking University, Beijing 100871, China

<sup>2</sup>International Joint Laboratory for Regional Pollution Control, Ministry of Education, Beijing, 100816, China

<sup>3</sup>Laboratory for Modelling and Observation of the Earth System (LAMOS), Institute of Environmental Physics (IUP), University of Bremen, Bremen, Germany

<sup>4</sup>Center of Marine Environmental Sciences (MARUM), University of Bremen, Germany

<sup>5</sup>Climate and Atmosphere Research Center (CARE-C), The Cyprus Institute, Cyprus

<sup>6</sup>State Key Laboratory of Regional Air Quality Monitoring, Guangdong Key Laboratory of Secondary Air Pollution Research, Guangdong Environmental Monitoring Center, Guangzhou 510308, China

<sup>7</sup>Beijing Innovation Center for Engineering Science and Advanced Technology, Peking University, Beijing 100871, China

<sup>8</sup>CAS Center for Excellence in Regional Atmospheric Environment, Chinese Academy of Sciences, Xiamen 361021, China

*Correspondence to:* Xuesong Wang (xswang@pku.edu.cn) and Yuanhang Zhang (yhzhang@pku.edu.cn)

## Contents

Three texts, ten figures and two tables are included in this Supporting Information for the paper entitled “Rethinking the role of transport and photochemistry in regional ozone pollution: Insights from ozone mass and concentration budgets”.

### For texts:

- Text S1 describes the detailed processes of O<sub>3</sub> budget calculations in this study.
- Text S2 compares the equations of O<sub>3</sub> budget calculations used in this study with these in 1-D models.
- Text S3 presents the results of model validation of atmospheric boundary layer (ABL) height, wind and O<sub>3</sub> mixing profiles based on the IAGOS dataset.

### For figures:

- Figure S1 indicates two calculation paths for the regional O<sub>3</sub> concentration budget within an hour.
- Figure S2 displays the spatial distributions of the second modelling domain (d02) and source regions.
- Figure S3 presents the spatial distributions of 18 sites of the Guangdong-Hong Kong-Macao Pearl River Delta (PRD) Regional Air Quality Monitoring Network.
- Figure S4 compared the mean diurnal changes of O<sub>3</sub> concentrations in the PRD from three sources: observational near-ground O<sub>3</sub> concentrations, modelled near-ground O<sub>3</sub> concentrations and ABL-mean O<sub>3</sub> concentrations.
- Figure S5 compares IAGOS and modelling wind roses in Hong Kong in the two representative months.
- Figure S6 displays the spatial distributions of mean contributions of vertical exchange near the ABL top due to large-scale air motion (ABLex-M) to O<sub>3</sub> mass changes in the morning and afternoon of two representative months.
- Figure S7 compares IAGOS and CMAQ modelling vertical profiles of O<sub>3</sub> mixing ratios in Hong Kong in the two representative months.
- Figure S8 is the flow diagram of the O<sub>3</sub> budget calculation processes.
- Figure S9 is the flow diagram of the O<sub>3</sub> budget calculation in Step I (or the post-processing tool *flux\_4d\_cal*).
- Figure S10 shows the comparison results between IAGOS and modelling atmospheric boundary layer height in Hong Kong in Oct. 2015.

### For tables:

- Table 1 gives more detailed information on the O<sub>3</sub> polluted days of the PRD in the two representative months.
- Table 2 lists the formulas in the O<sub>3</sub> budget calculations, the parameters used and their corresponding source files in the *flux\_4d\_cal* tool.

## Text S1. Detailed processes of O<sub>3</sub> budget calculations

As the flow diagram shown in Fig. S8, there are two steps in the calculations of O<sub>3</sub> budgets based on the WRF-CMAQ modelling results:

### 1) Step I: Quantifications of transport fluxes and volume

The post-processing tool *flux\_4d\_cal* was developed using FORTRAN90 for this step. For all grid columns except for those next to the boundaries of the modelling domain, the calculation contents in the tool include:

- Hourly contributions of horizontal transport to O<sub>3</sub> mass changes within the ABL, including these in the x- and y-directions;
- Hourly contributions of vertical exchange due to the changes of ABL height (ABLex-H) to O<sub>3</sub> mass changes within the ABL;
- Hourly contributions of vertical exchange due to large-scale air motion (ABLex-M) to O<sub>3</sub> mass changes within the ABL, including these in the x-, y- and z-directions;
- Hourly contributions of other processes (gas-phase chemistry, cloud process and dry deposition) to O<sub>3</sub> mass changes within the ABL;
- Hourly transported air volumes by each transport process;
- Total O<sub>3</sub> masses within the ABL at both the start and end of each hour;
- ABL heights at the starting and end hours.

All of the above values can be found in the NetCDF (nc) output files, and they are used in the Step II calculations.

To finish the calculations of Step I, several input files are needed:

- Meteorological files processed by the MCIP module in CMAQ from the WRF outputs, which include the METCRO2D (meteorological parameters in the 2-D space), METCRO3D (meteorological parameters in the 3-D space) and MERDOT3D (wind speeds in the 3-D space) files;
- Pollutant concentration output files (CONC files) modelled by CMAQ, where hourly O<sub>3</sub> concentrations are stored;
- Process Analysis (PA) output files modelled by CMAQ, where the hourly, nested contributions of gas-phase chemistry, cloud process and dry deposition to O<sub>3</sub> concentration are stored.

For most of the files used here, the setting of spatial domains and times should be consistent; otherwise, the calculations would not be performed or generate wrong results. Additionally, users should provide the resolution of the modelling domain and the orders of contributions by three non-transport O<sub>3</sub> processes in the PA files for further calculations.

The flow chart of the calculation in *flux\_4d\_cal* is shown in Fig. S9. The calculation formulas for the grid column (*i, j*), parameters used and their source files are summarized in Table S2. There are four loops in the calculations, which are the

loops of x-, y-grids, time steps and vertical layers. We assume that there are 60 time-steps within an hour, and parameters at each time step can be interpolated linearly by their values at the starting and end hours. The hourly contribution of non-transport processes to  $O_3$  in a grid cell is divided equally to these within each time step. For every layer within the ABL, fluxes and volumes related to horizontal transport and non-transport processes are calculated and summed up. For layers where the ABL top is located, besides these aforementioned parameters, contributions to  $O_3$  mass changes and volumes related to vertical exchange (ABLex-H and ABLex-M) are also calculated. Total  $O_3$  masses within the ABL at the start and end of each hour are directly calculated, and ABL heights at the starting and end hours can be read from the METCRO2D files.

The height of night-time stable ABL can be severely underestimated by normally used ABL parameterization, especially when the Richardson number is used (Dai et al., 2014). To reduce the influence of imprecise ABL heights in the  $O_3$  budget calculations, here, we set the lowest ABL height limit as 350 m for all hours, which is an approximate value close to the values reported by night-time observations in summer or autumn in the Pearl River Delta (Chan et al., 2006; Fan et al., 2011; He et al., 2021; Song et al., 2021). The results of the budget closure examination (Fig. 2 in the manuscript) also suggest that the choice of this value is acceptable. Further studies are surely needed to determine this value better. However, we focus on the causes of daytime ozone pollution; thus, night-time budgets do not notably influence the conclusions of this study.

## 2) Step II: Regional $O_3$ budget calculations and closure examinations

This step aims to: 1) calculate the hourly  $O_3$  mass and concentration budgets within the ABL of the user-defined regions and 2) check whether the closure between the changes of  $O_3$  masses/concentrations modelled by CMAQ and the net contributions of processes calculated above can be achieved. Besides the nc file generated in Step I, the definition of targeted region grids and borders (the grids within the targeted region and adjacent to the outside regions) should also be provided by the users. Any software with basic data analysis and nc-file processing (Python, MATLAB, R, etc.) functions can be applied for this step.

The calculation processes in this step include:

- Calculation of hourly contributions of horizontal transport to  $O_3$  mass changes through each user-defined border (horizontal transport contributions in every interface between the border grids and the outside regions, in both x- and y-directions, are taken into the calculations).
- Calculation of hourly contributions of vertical exchange near the ABL top to  $O_3$  mass changes as well as the contributions of other processes within user-defined targeted region grids.
- Calculation of the hourly  $O_3$  concentration budget (the contributions of processes to the hourly variations of  $O_3$  concentrations) based on transport contributions to  $O_3$  mass changes and the corresponding volumes of transported air parcels.

More details on the calculation of the  $O_3$  concentration budget are introduced as follows. As displayed in Fig. S1, within an hour, the mean  $O_3$  concentration within the ABL of the targeted region changes from  $c_0$  to  $c_1$ . Normally,  $O_3$  mass and ABL volume both change notably, making it difficult to quantify the contributions to  $O_3$  concentration variations by various processes. It should be noted that this is also one of the main reasons why the regional  $O_3$  mass and concentration budgets are different. To simplify the calculation, two calculation paths (shown as the red arrow lines in Fig. S1;  $c_{r1}$  and  $c_{r2}$  are the reference  $O_3$  concentrations separately for two calculation paths) are used in the calculations, assuming that only  $O_3$  mass or ABL volume change in each step of two paths. For the path “ $c_0 \Rightarrow c_{r1} \Rightarrow c_1$ ”, the first step is the ABL volume change step, with  $O_3$  concentration change described as:

$$c_{r1} - c_0 = c_0 \times \left( \frac{\sum H_0}{\sum H_1} - 1 \right) \quad (S1)$$

where  $H_0$  and  $H_1$  are the ABL heights at the starting and end hours. It is counted as part of the contributions by ABLex-H.

The second step is the  $O_3$  mass change step, with  $O_3$  concentration change described as:

$$c_1 - c_{r1} = \frac{\sum(F_{\text{htrans}} - c_{r1} \times \Delta V_{\text{htrans}})}{L^2 \times \sum H_1} + \frac{\sum(F_{\text{ABLex-M}} - c_{r1} \times \Delta V_{\text{ABLex-M}})}{L^2 \times \sum H_1} + \frac{F_{\text{ABLex-H}}}{L^2 \times \sum H_1} \\ + \frac{F_{\text{chem}}}{L^2 \times \sum H_1} + \frac{F_{\text{cloud}}}{L^2 \times \sum H_1} + \frac{F_{\text{ddep}}}{L^2 \times \sum H_1} \quad (S2)$$

where  $F_{\text{htrans}}$ ,  $F_{\text{ABLex-M}}$ ,  $F_{\text{ABLex-H}}$ ,  $F_{\text{chem}}$ ,  $F_{\text{cloud}}$  and  $F_{\text{ddep}}$  indicate the contributions of horizontal transport, ABLex-M, ABLex-H, gas-phase chemistry, cloud process and dry deposition, respectively, to  $O_3$  mass changes.  $\Delta V_{\text{htrans}}$  and  $\Delta V_{\text{ABLex-M}}$  are the volumes of transported air parcels attributed to horizontal transport and ABLex-M, respectively, within an hour.  $L$  denotes the length of the grid cell, or the horizontal resolution of the model. The six terms on the right-hand side of the above formula are separately classified as the individual contribution of horizontal transport, ABLex-M, ABLex-H, gas-phase chemistry, cloud process and dry deposition in the  $O_3$  concentration budgets. Note that the contributions of ABLex-H are separately calculated in two steps. Similarly, for the path “ $c_0 \Rightarrow c_{r2} \Rightarrow c_1$ ”, the changes in  $O_3$  concentration in two steps can be described as:

$$c_{r2} - c_0 = \frac{\sum(F_{\text{htrans}} - c_0 \times \Delta V_{\text{htrans}})}{L^2 \times \sum H_0} + \frac{\sum(F_{\text{ABLex-M}} - c_0 \times \Delta V_{\text{ABLex-M}})}{L^2 \times \sum H_0} + \frac{F_{\text{ABLex-H}}}{L^2 \times \sum H_0} \\ + \frac{F_{\text{chem}}}{L^2 \times \sum H_0} + \frac{F_{\text{cloud}}}{L^2 \times \sum H_0} + \frac{F_{\text{ddep}}}{L^2 \times \sum H_0} \quad (S3)$$

$$c_1 - c_{r2} = c_{r2} \times \left( \frac{\sum H_0}{\sum H_1} - 1 \right) \quad (S4)$$

The contributions of various processes can be classified correspondingly. The final results of contributions by processes are the average values of these calculated based on two calculation paths.

## Text S2. Comparisons of the O<sub>3</sub> concentration budget calculations between this study and 1-D models

When the region column in the Chemical Transport Models (CTMs) is thin enough to resemble a line, the O<sub>3</sub> concentration budget calculations using the CTMs results are expected to be the same as those in 1-D models. Thus, we can use it to check the validity of the O<sub>3</sub> concentration budget calculations in this study.

Here the contributions of horizontal transport to the variations of O<sub>3</sub> concentration over the studied space ( $\langle c \rangle$ ) can be described as (Eq. (6) in the manuscript):

$$\left[ \frac{\partial \langle c \rangle}{\partial t} \right]_{htrans} = \frac{F_{htrans} + \langle c \rangle(V - dV)}{V} - \langle c \rangle = \frac{F_{htrans} - \langle c \rangle dV}{V} \quad (S5)$$

where  $F_{htrans}$  is the contributions of horizontal transport to O<sub>3</sub> mass changes;  $V$  is the original volume of the PRD grids below the ABL;  $dV$  is the volume of transported parcels. Assume that the length of the region in the x-directions is  $dx$ , thus,

$$V = S dx \quad (S6)$$

where  $S$  is the area of the interface. As calculated in the O<sub>3</sub> mass budget, in the unit time,

$$F_{htrans} = cuS \quad (S7)$$

$$dV = uS \quad (S8)$$

where  $c$  is the O<sub>3</sub> concentration in the transported air parcels, and  $u$  is the mean horizontal wind speed in the interface.

Therefore, from Eqs. (S5)-(S8), we can get:

$$\left[ \frac{\partial \langle c \rangle}{\partial t} \right]_{htrans} = u \frac{c - \langle c \rangle}{dx} = u \frac{dc}{dx} \quad (S9)$$

For ABLex-H, its contributions when  $V$  is much higher than  $dV$  (this assumption can be normally met when the period is short) are:

$$\left[ \frac{\partial \langle c \rangle}{\partial t} \right]_{ABLex-H} = \frac{F_{ABLex-H} + \langle c \rangle V}{V + dV} - \langle c \rangle \approx \frac{F_{ABLex-H} - \langle c \rangle dV}{V} \quad (S10)$$

where  $F_{ABLex-H}$  is the O<sub>3</sub> mass change attributed to ABLex-H. In the unit time,

$$F_{ABLex-H} = c_h \frac{\partial H}{\partial t} L^2 \quad (S11)$$

$$dV = \frac{\partial H}{\partial t} L^2 \quad (S12)$$

$$V = HL^2 \quad (S13)$$

where  $c_h$  is the O<sub>3</sub> concentration in the ABL top;  $L$  is the width of the grid cell (equal to the horizontal resolution of the model);  $H$  is the ABL height. Therefore, from Eqs. (S10)-(S13),

$$\left[ \frac{\partial \langle c \rangle}{\partial t} \right]_{ABLex-H} = \frac{c_h - \langle c \rangle}{H} \frac{\partial H}{\partial t} \quad (S14)$$

For ABLex-M,

$$\left[ \frac{\partial \langle c \rangle}{\partial t} \right]_{ABLex-M} = \frac{F_{ABLex-M} + \langle c \rangle (V - dV)}{V} - \langle c \rangle = \frac{F_{ABLex-M} - \langle c \rangle dV}{V} \quad (S15)$$

$F_{ABLex-M}$  is the  $O_3$  flux attributed to ABL-FT-M. In the unit time,

$$F_{ABLex-M} = c_h \left( u_h \frac{\partial H}{\partial x} + v_h \frac{\partial H}{\partial y} - w_h \right) L^2 \quad (S16)$$

$$dV = \left( u_h \frac{\partial H}{\partial x} + v_h \frac{\partial H}{\partial y} - w_h \right) L^2 \quad (S17)$$

$$V = HL^2 \quad (S18)$$

where  $u_h$ ,  $v_h$  and  $w_h$  are the ABL-top wind speeds in the x, y and z-direction, respectively. Therefore, from Eq. (S15-18),

$$\left[ \frac{\partial \langle c \rangle}{\partial t} \right]_{ABLex-M} = \frac{c_h - \langle c \rangle}{H} \left( u_h \frac{\partial H}{\partial x} + v_h \frac{\partial H}{\partial y} - w_h \right) \quad (S19)$$

$$\begin{aligned} \left[ \frac{\partial \langle c \rangle}{\partial t} \right]_{ABLex} &= \left[ \frac{\partial \langle c \rangle}{\partial t} \right]_{ABLex-H} + \left[ \frac{\partial \langle c \rangle}{\partial t} \right]_{ABLex-M} = \frac{c_h - \langle c \rangle}{H} \left( \frac{\partial H}{\partial t} + u_h \frac{\partial H}{\partial x} + v_h \frac{\partial H}{\partial y} - w_h \right) \\ &= \frac{w_e \Delta c}{H} \end{aligned} \quad (S20)$$

where  $w_e$  is the entrainment rate of the ABL;  $\Delta c$  is equal to the difference between  $O_3$  concentrations above and within the ABL. Therefore, for these transport processes, the above formulas (Eqs. (S9), (S14), (S19), and (S20)) are the same as those used in 1-D models (Janssen and Pozzer, 2015; Vilà-Guerau de Arellano et al., 2015), suggesting their applicability in the quantification of the  $O_3$  concentration budget using CTMs modelling results.

### **Text S3. Model validation of ABL height, wind and O<sub>3</sub> mixing ratio profiles based on the IAGOS dataset**

IAGOS (In-service Aircraft of a Global Observing System; <https://www.iagos.org>) is a global aircraft-based observing system, where state-of-the-art instruments deployed in aircraft are used to measure reactive gases, greenhouse gases, aerosol and clouds in the troposphere and lower stratosphere (Petzold et al., 2016). Meteorological parameters, including air temperature, wind speed and direction, are also provided by IAGOS. When the aircraft climb up or descend, these measurements are suitable for obtaining the vertical profiles of parameters with high resolutions, which provides valuable observational datasets for the model validation in the vertical direction.

To ensure reasonable quantifications of the O<sub>3</sub> budgets, the IAGOS dataset in two representative months in Hong Kong (located in the south PRD) was used to evaluate the modelling performance of WRF-CMAQ in this study. We focused on comparing parameters within the height range of 0-5 km. Since observational data is often missing in some height ranges and the vertical resolution of modelling results is relatively low, we calculated the mean observational and modelling values within every 500 m height range (i.e., 0-500 m, 500-1000 m, etc.) for the comparisons. The detailed evaluations are introduced as follows:

#### **(1) Atmospheric boundary layer (ABL) heights:**

ABL heights are used to quantify the contribution of vertical exchange near the ABL top in the O<sub>3</sub> budgets. Therefore, the evaluation of modelled ABL heights is important. In this study, the observational ABL heights were determined using the profiles of potential temperature ( $\theta$ ) in IAGOS, defined as the heights where the lapse rate of  $\theta$  ( $\partial\theta/\partial z$ , the rate of  $\theta$  changing over height change) reaches its maximum values (Dai et al., 2014). Since there are limited profiles available in July 2016 and night-time ABL heights are hard to determine accurately, we only evaluated the modelling performance of ABL heights during the daytime (6:00-18:00 Local Time (LT)) of Oct. 2015. As shown in Fig. S10, the mean bias (MB) between modelling and observational ABL heights in Hong Kong is only -1.1 m, and a good correlation between ABL heights from two datasets ( $R = 0.76$ ) suggests that the mean diurnal cycles of ABL can be modelled well. Though the modelling performance of ABL heights is satisfying based on the IAGOS dataset in Hong Kong, more comprehensive comparisons based on three-dimensional observations with higher spatiotemporal resolutions and coverages are required for more accurate O<sub>3</sub> budget estimates in future studies.

#### **(2) Wind profiles:**

Figure S5 shows the IAGOS and modelling wind roses within the height ranges of 0-1000 m, 1000-2000 m and 2000-5000 m. Both datasets indicate that higher wind speeds can be generally found at higher altitudes. In autumn, WRF overestimates wind speed below 1000 m by 0.6 m/s (16%) but underestimates it above 1000 m. In summer, the biases between wind speeds in the two datasets are relatively smaller, especially at lower heights (< 2000 m). Both datasets show similar prevailing wind



directions at different height ranges and seasons. Thus, the modelling performance of wind speeds and directions in the vertical direction is acceptable.

### **(3) O<sub>3</sub> mixing ratio profiles:**

The comparisons between observational and modelling profiles of the O<sub>3</sub> mixing ratio are displayed in Fig. S7. Few O<sub>3</sub> profiles were available in July 2016, and the useable ones were mostly measured during clean periods. Thus, the comparison was mainly based on the results in Oct. 2015 (the number of IAGOS O<sub>3</sub> profiles available for the comparisons is 41). Both datasets show that the O<sub>3</sub> mixing ratio decreases with height in Hong Kong. Below the height of 1000 m, the observational and modelling O<sub>3</sub> mixing ratios are 71.4 ppbv and 75.8 ppbv, respectively. Within the height range of 1000-2000 m, the O<sub>3</sub> mixing ratio is overestimated by 26%. High O<sub>3</sub> levels during Oct. 13-24 and relatively low O<sub>3</sub> levels in other periods can be found in both datasets, suggesting that the developments of O<sub>3</sub> pollution in the month were modelled well. Therefore, the performance of O<sub>3</sub> profile modelling can also meet the requirement of O<sub>3</sub> budget calculations.

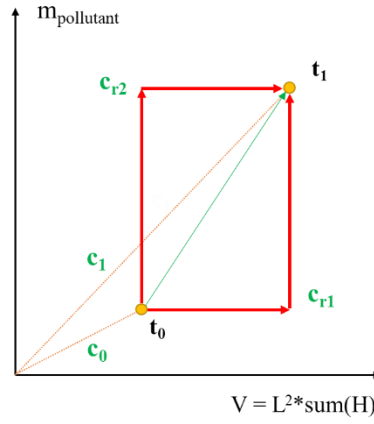


**Figure S1.** Two calculation paths for the regional O<sub>3</sub> concentration budget within an hour.  $m_{\text{pollutant}}$  indicates the total mass of pollutants in the atmospheric boundary layer (ABL) of the studied region;  $V$  is the volume of the ABL of the region;  $L$  is the length of the grids (equal to the horizontal resolution of the model);  $H$  is the ABL heights;  $t_0$  and  $t_1$  are the starting and end hours;  $c_0$  and  $c_1$  are the concentrations of pollutants in  $t_0$  and  $t_1$ , respectively;  $c_{r1}$  and  $c_{r2}$  are the reference concentrations of pollutants for two calculation paths.

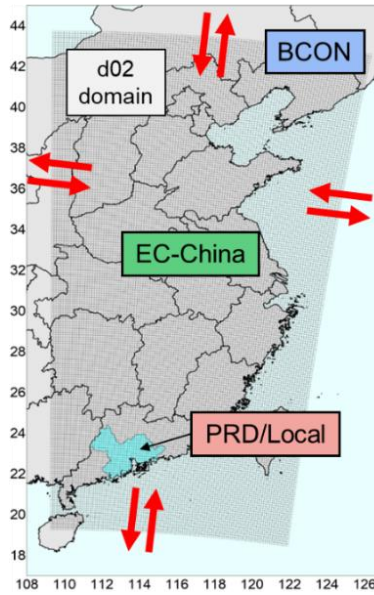


**Figure S2.** The spatial distributions of the d02 modelling domain and source regions. PRD, Pearl River Delta; EC-China, East and Central China; BCON, the boundary conditions of d02 modelling, or the contributions of sources outside d02.

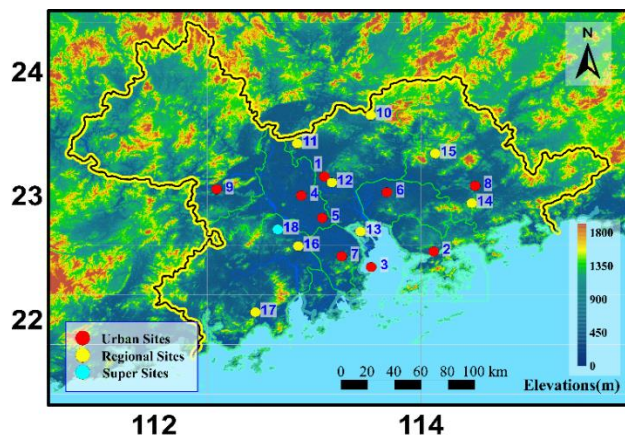


**Figure S3.** Spatial distributions of 18 sites of the Guangdong-Hong Kong-Macao Pearl River Delta Regional Air Quality Monitoring Network. The names of all sites and their located municipalities are: 1. Luhu, Guangzhou; 2. Liyuan, Shenzhen; 3. Tangjia, Zhuhai; 4. Huijingcheng, Foshan; 5. Jinjuju, Foshan; 6. Nanchengyuanling, Dongguan; 7. Zimaling, Zhongshan; 8. Xiapu, Huizhou; 9. Chengzhongzizhan, Zhaoqing; 10. Tianhu, Guangzhou; 11. Zhudong, Guangzhou; 12. Modiesha, Guangzhou; 13. Wanqingsha, Guangzhou; 14. Jinguowan, Huizhou; 15. Xijiao, Huizhou; 16. Donghu, Jiangmen; 17. Duanfen, Jiangmen; 18. Heshan Supersite, Jiangmen.

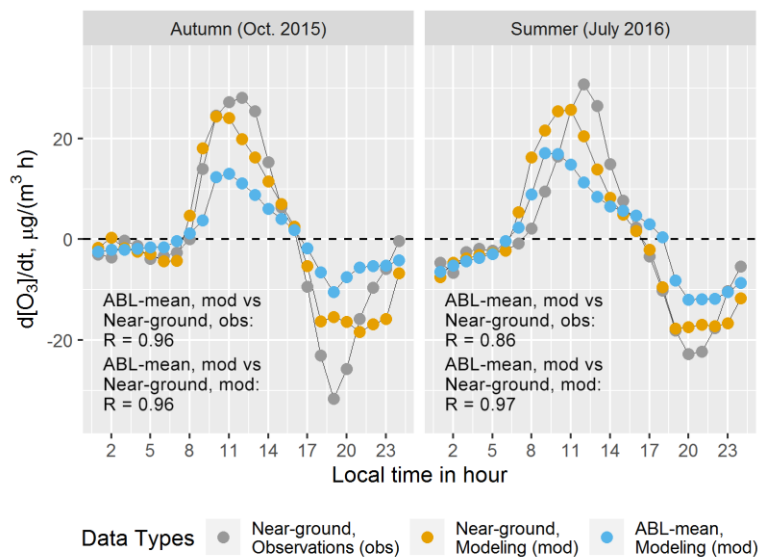


**Figure S4.** Mean diurnal change of the hourly variations of observational, modelling mean near-ground  $O_3$  concentrations in 18 sites of the Guangdong-Hong Kong-Macao regional monitoring network and modelling mean  $O_3$  concentration over the atmospheric boundary layer (ABL) of the Pearl River Delta on the polluted days of autumn (Oct. 2015) and summer (July 2016).

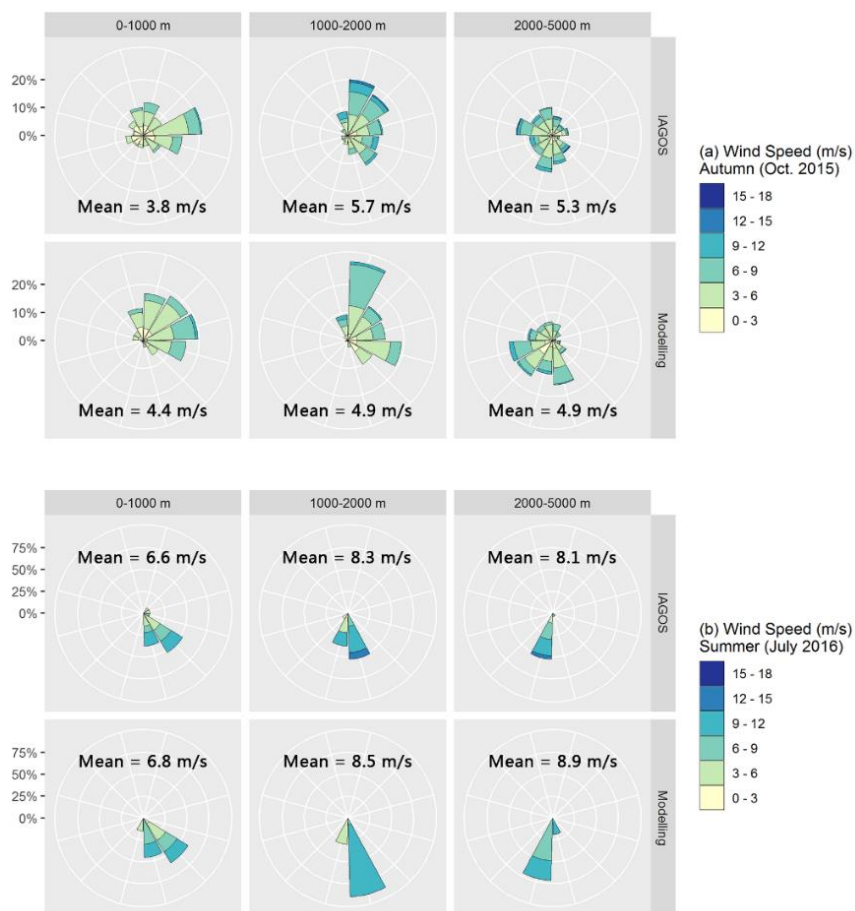


**Figure S5.** Comparisons between IAGOS and modelling wind roses in Hong Kong in (a) Oct. 2015 and (b) July 2016. Results within the height range of 0-1000 m, 1000-2000 m, and 2000-5000 m were separately displayed.

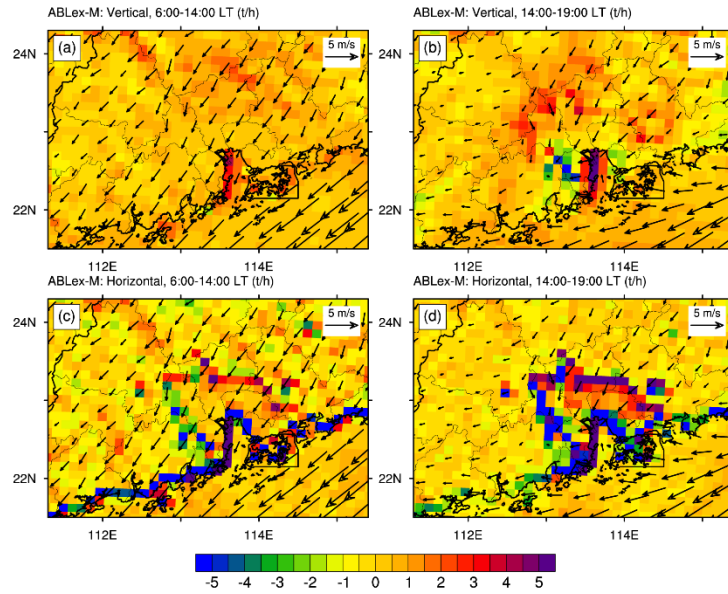


**Figure S6.** The spatial distributions of contributions of ABLex-M to  $O_3$  mass changes on the polluted days of Oct. 2015. (a-b) Contributions through vertical advection; (c-d) contributions through horizontal advection. (a,c) The mean results during the morning hours (6:00-14:00 LT); (b,d) the mean results during the afternoon hours (14:00-19:00 LT).

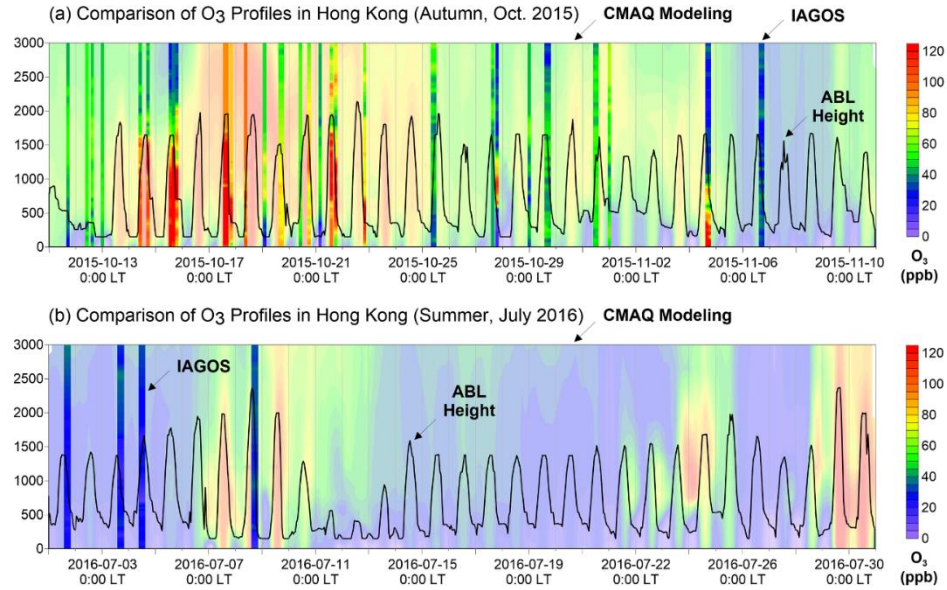


**Figure S7.** Comparisons between IAGOS and CMAQ modelling vertical profiles of  $O_3$  mixing ratios (ppb) in Hong Kong in (a) Oct. 2015 and (b) July 2016. The heights of the atmospheric boundary layer (ABL) modelled by WRF in two months are also shown as solid black lines.

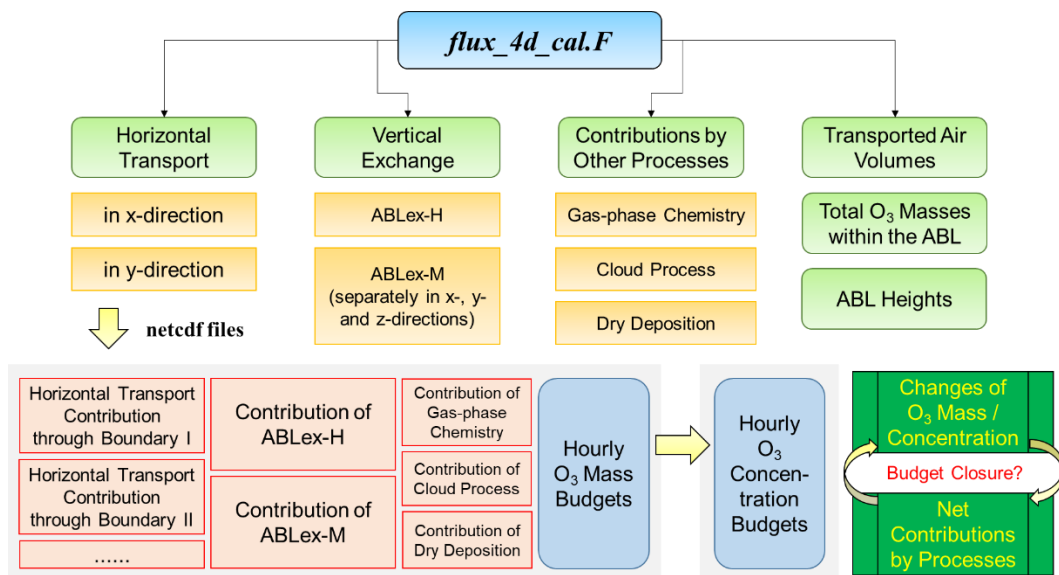


**Figure S8.** Flow diagram of the O<sub>3</sub> budget calculation processes. ABL, atmospheric boundary layer; ABLeX-H, vertical exchange near the ABL top due to the changes of ABL height; ABLeX-M, vertical exchange near the ABL top due to the large-scale air motions (advection through the ABL top).

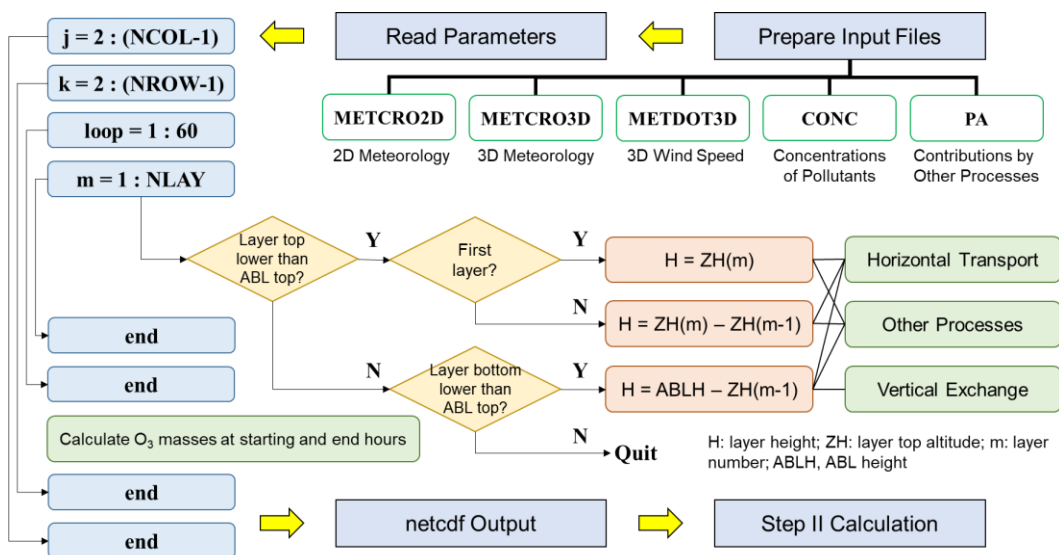


**Figure S9.** Flow diagram of the O<sub>3</sub> budget calculation in Step I (or the post-processing tool *flux\_4d\_cal*). NCOL, NROW and NLAY indicate the number of columns, rows and vertical layers in the modelling domain. ABL, atmospheric boundary layer. METCRO2D, 2-dimensional meteorological outputs from the MCIP module in CMAQ; METCRO3D, 3-dimensional meteorological outputs from the MCIP module in CMAQ; METDOT3D, 3-dimensional wind fields outputs from the MCIP module in CMAQ; CONC, 3-dimensional outputs of pollutant concentrations from CMAQ; PA, 3-dimensional outputs of hourly contributions by three non-transport processes to O<sub>3</sub> from CMAQ.

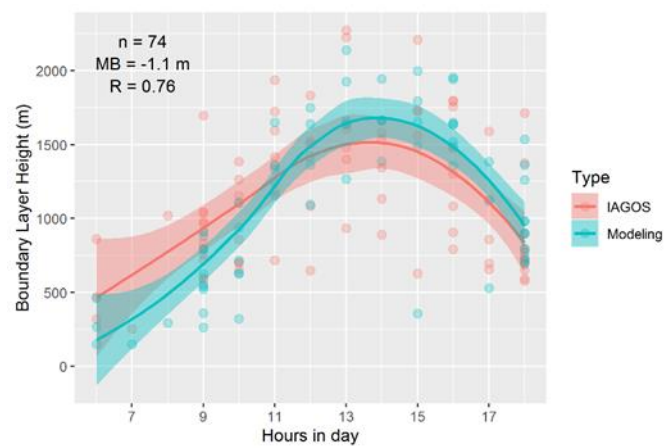


**Figure S10.** Comparisons between IAGOS and modelling atmospheric boundary layer height in Hong Kong in Oct. 2015.  $n$ , the number of the available dataset for the comparison; MB, mean bias;  $R$ , correlation factor.

**Table S1.** Information on the O<sub>3</sub> polluted days of the Pearl River Delta (PRD) in Oct. 2015 and July 2016. MDA1, the maximum 1-hr O<sub>3</sub> concentrations; MDA8, the maximum 8-hr average O<sub>3</sub> concentrations.

Dates	Influencing Weather Systems	O <sub>3</sub> concentrations in the PRD (the maximum values in nine municipals of the PRD, released by the China National Environmental Monitoring Centre; µg/m <sup>3</sup> )	
		MDA1	MDA8
Oct.13, 2015	Typhoon Koppu and Champi	201	164
Oct.14, 2015		301	244
Oct.15, 2015		271	227
Oct.16, 2015		260	219
Oct.17, 2015		233	211
Oct.18, 2015		205	187
Oct.19, 2015		214	174
Oct.20, 2015		200	158
Oct.21, 2015		214	195
Oct.22, 2015		209	182
Oct.23, 2015		249	199
Oct.24, 2015		225	193
Oct.28, 2015	Subtropical High	238	186
Nov.3, 2015	Sea High	207	162
Nov.4, 2015		182	168
Nov.5, 2015		255	187
July 7, 2016	Typhoon Nepartak	297	256
July 8, 2016		260	198
July 9, 2016		263	231
July 10, 2016		211	150
July 22, 2016	Subtropical High	211	176
July 23, 2016		223	197
July 24, 2016		265	226
July 25, 2016		334	269
July 26, 2016		235	164
July 29, 2016		271	204
July 30, 2016	Typhoon Nida	268	187
July 31, 2016		385	344



**Table S2.** Formulas in the calculations of contributions to O<sub>3</sub> mass changes for the grid cell  $(i, j)$  in the unit time  $dt$ , parameters used and their source files in the *flux\_4d\_cal* tool.

Processes	Formulas of O <sub>3</sub> fluxes	Parameters used	Sources of parameters
Horizontal transport (in the x-direction)	$F_{u-trans} = \sum_{k=1}^h c_{i-1,j} u_{i,j+\frac{1}{2}} L \Delta z dt$	$c_{i-1,j}$ : O <sub>3</sub> concentrations in the grid cell $(i-1, j)$	CONC files
		$u_{i,j+\frac{1}{2}}$ : wind speeds in the west interface	METD0T3D files
		$L$ : the length of grid cells (= model resolution)	User defined
		$\Delta z$ : layer heights $(H - z_{h-1}$ for the ABL top layer, $z_k - z_{k-1}$ for other layers within the ABL; H, ABL height)	METCRO3D files
		h: the layer of ABL top	Determined by ABL height
Horizontal transport (in the y-direction)	$F_{v-trans} = \sum_{k=1}^h c_{i,j-1} v_{i+\frac{1}{2},j} L \Delta z dt$	$c_{i,j-1}$ : O <sub>3</sub> concentrations in the grid cell $(i, j-1)$	CONC files
		$v_{i+\frac{1}{2},j}$ : wind speeds in the south interface	METD0T3D files
		$L$ : the length of grid cells (= model resolution)	User defined
		$\Delta z$ : layer heights $(H - z_{h-1}$ for the ABL top layer, $z_k - z_{k-1}$ for other layers within the ABL; H, ABL height)	METCRO3D files
		h: the layer of ABL top	Determined by ABL height
ABL <sub>ex</sub> -H	$F_{ABL\text{ex}-H} = c_h \frac{\partial H}{\partial t} L^2 dt$	$c_h$ : O <sub>3</sub> concentrations in the ABL top layer	CONC files
		$\frac{\partial H}{\partial t}$ : the change rates of ABL height	METCRO2D files
		$L$ : the length of grid cells (= model resolution)	User defined
		$c_{i-1,j}(h)$ : O <sub>3</sub> concentrations in the ABL top layer of the grid cell $(i-1, j)$	CONC files
		$u_{i,j+\frac{1}{2}}(h)$ : wind speeds in the ABL top layer of the west interface	METD0T3D files
ABL <sub>ex</sub> -M (in the x-direction)	$F_{ABL\text{ex}-Mx} = c_{i-1,j}(h) u_{i,j+\frac{1}{2}}(h) \frac{\partial H}{\partial x} L^2 dt$	$L$ : the length of grid cells (= model resolution)	User defined
		$\frac{\partial H}{\partial x}$ : the difference of ABL heights in x-direction, or between the grid cells $(i, j)$ and $(i-1, j)$	METCRO2D files
		$c_{i,j-1}(h)$ : O <sub>3</sub> concentrations in the ABL top layer of the grid cell $(i, j-1)$	CONC files
		$v_{i+\frac{1}{2},j}(h)$ : wind speeds in the ABL top layer of the south interface	METD0T3D files
		$L$ : the length of grid cells (= model resolution)	User defined
ABL <sub>ex</sub> -M (in the y-direction)	$F_{ABL\text{ex}-My} = c_{i,j-1}(h) v_{i+\frac{1}{2},j}(h) \frac{\partial H}{\partial y} L^2 dt$	$\frac{\partial H}{\partial y}$ : the difference of ABL heights in y-direction, or between the grid cells $(i, j)$ and $(i, j-1)$	METCRO2D files
		$c_h$ : O <sub>3</sub> concentrations in the ABL top layer	CONC files
		$w_h$ : vertical wind speeds in the ABL top layer	METCRO3D files
		$L$ : the length of grid cells (= model resolution)	User defined
		$IPR$ : integrated process rates of pre-set processes	PA files
Other processes (gas-phase chemistry, cloud process, dry deposition)	$F_{others} = \sum_{k=1}^h IPR \Delta z dt$	$\Delta z$ : layer heights $(H - z_{h-1}$ for the ABL top layer, $z_k - z_{k-1}$ for other layers within the ABL; H, ABL height)	METCRO3D files
		h: the layer of ABL top	Determined by ABL height

## References (of the Supplement)

- Chan, R. L. M., Lee, O. S. M., and Cheng, A. Y. S.: Diurnal variation of mixing height in Hong Kong. In Reviewed and revised papers presented at the 23rd International Laser Radar Conference (pp. 737-740), 2006.
- Dai, C., Wang, Q., Kalogiros, J. A., Lenschow, D. H., Gao, Z., and Zhou, M.: Determining Boundary-Layer Height from Aircraft Measurements, *Bound.-Lay. Meteorol.*, 152, 277–302, <https://10.1007/s10546-014-9929-z>, 2014.
- Fan, S. J., Fan, Q., Yu, W., Luo, X. Y., Wang, B. M., Song, L. L., and Leong, K. L.: Atmospheric boundary layer characteristics over the Pearl River Delta, China, during the summer of 2006: measurement and model results, *Atmos. Chem. Phys.*, 11, 6297–6310, <https://doi.org/10.5194/acp-11-6297-2011>, 2011.
- He, G., Deng, T., Wu, D., Wu, C., Huang, X., Li, Z., Yin, C., Zou, Y., Song, L., Ouyang, S., Tao, L., and Zhang, X.: Characteristics of boundary layer ozone and its effect on surface ozone concentration in Shenzhen, China: A case study, *Sci. Total Environ.*, 791, 148044, <https://doi.org/10.1016/j.scitotenv.2021.148044>, 2021.
- Janssen, R. H. H. and Pozzer, A.: Description and implementation of a MiXed Layer model (MXL, v1.0) for the dynamics of the atmospheric boundary layer in the Modular Earth Submodel System (MESSy), *Geosci. Model Dev.*, 8, 453–471, <https://doi.org/10.5194/gmd-8-453-2015>, 2015.
- Petzold, A., Thouret, V., Gerbig, C., Zahn, A., Brenninkmeijer, C. A. M., Gallagher, M., Hermann, M., Pontaud, M., Ziereis, H., Boulanger, D., Marshall, J., Nédélec, P., Smit, H. G. J., Friess, U., Flaud, J.-M., Wahner, A., Cammas, J.-P., Volz-Thomas, A. and IAGOS TEAM: Global-scale atmosphere monitoring by in-service aircraft—current achievements and future prospects of the European Research Infrastructure IAGOS, *Tellus B*, 67, 28452, <https://doi.org/10.3402/tellusb.v67.28452>, 2015.
- Song, L., Deng, T., Li, Z. N., Wu, C., He, G. W., Li, F., Wu, M., and Wu, D. (2021). Retrieval of boundary layer height and its influence on PM<sub>2.5</sub> concentration based on lidar observation over Guangzhou, *J. Trop. Meteorol.*, 27(3), 303-318, <https://doi.org/10.46267/j.1006-8775.2021.027>, 2021.
- Vilà-Guerau De Arellano, J., van Heerwaarden, C. C., van Stratum, B. J. H., and van den Dries, K.: *Atmospheric Boundary Layer: Integrating Air Chemistry and Land Interactions*, Cambridge University Press, New York, 2015.